Dimitar Dichev ✉
Iliya Zhelezarov
Nikolay Madzharov

https://doi.org/10.21278/TOF.454029721
ISSN 1333-1124
eISSN 1849-1391

DYNAMIC ERROR AND METHODS FOR ITS ELIMINATION IN SYSTEMS FOR MEASURING PARAMETERS OF MOVING OBJECTS

Summary

This paper presents a new block diagram for defining a dynamic error in instruments for measuring the angular position of moving objects. The diagram proposes a new concept for investigating dynamic error characteristics as well as for compiling algorithms, inventing methods, and employing means for elimination of the dynamic error as independent component. Based on that concept, a system for measuring the roll, pitch, trim, and heel of moving objects has been developed. The system features high accuracy ensured through a combination of the capacities of different micro-electromechanical sensors that are unified into a shared platform with a specific algorithm used to determine and eliminate a real-time dynamic error. In addition, the paper presents the results from experimental research work. The results confirm the large operational capacity of the proposed concept concerning measurement accuracy.

Key words: *dynamic error, micro-electromechanical system, error analysis, error correction*

1. Introduction

Undoubtedly, tasks related to measurement accuracy and its improvement is among the ones underlying the development of measuring instruments. Successful solution to these problems has always been one of the most important prerequisites for further improvement of measuring instruments, thereby contributing to a large extent to the overall development of many branches of science and technology which rely on accurate measurements. For example, accurate and timely information concerning the measurement of movement parameters will enable further improvement in modern means of transportation with regard to their control, maneuverability, low consumption rate, safety, comfort, etc. [1-4].

Alternatively, the accuracy of instruments in measuring parameters of moving objects is preconditioned most of all by the dynamic error value [5-8]. The latter is largely due to inertial effects related to the primary transducer as well as to some random noises being present in the measuring circuit of the instrument [9, 10]. Inertial effects are generated by the movement of moving objects and primarily, by the ships' trim and keel, oscillations of air-

crafts and ground vehicles as well as by the vibrations at the location where measuring instruments are placed [11-13].

Sensitive elements, which have been developed in accordance with gyroscope properties, are used in the existing measuring instruments for the purpose of increasing dynamic accuracy [14]. On the other hand, the measuring instruments built on the basis of gyro-verticals have a number of disadvantages, such as a complicated design, lower reliability under extreme conditions, a requirement for special systems ensuring the gyro-vertical operation, large sizes, and high prices [15-18]. Thus, their application is limited to a great extent.

A complete solution to these problems can be found by using the method proposed in this paper. Unlike existing methods and measuring instruments using the stabilisation of the vertical in inertial space, the proposed approach is based on a methodology that eliminates dynamic error in real time. The proposed concept for modelling measuring instruments and systems of this type overcomes, to a great degree, the disadvantages listed above. In this respect, micro-electromechanical systems (MEMS) appear to offer promising prospects and applications [19-21]. Independent use of individual sensors as primary transducers is, of course, quite limited due to a number of flaws and the heavy-duty mode of operation caused by inertial effects. In this respect, the combination of various sensors in one shared platform with an application-oriented algorithm for control and data processing will provide a far more accurate and reliable measuring output [22-26].

The integration of measuring instruments in that particular field with the advantages of modern computer systems and the introduction of algorithms for the optimized adaptation of dynamic parameters into a common concept, could substantially increase the accuracy of measurements, improve the metrological characteristics of measuring systems, and extend the scope of their functional possibilities. Accordingly, this paper proposes a new concept for the development of application-oriented sensor system which targets the dynamic error elimination in real time. At the core of this concept is the block diagram of dynamic error of instruments and systems for measuring the angular position of moving objects, which is presented in the following section.

2. Dynamic error

The basic dynamic error component is determined by the deviations of the sensitive element of the primary transducer and, also by its reference position which results from inertial effects on the spot where the instrument is fixed. Therefore, in the block diagram shown in Fig.1, the elements of the measuring instrument are structured, though conditionally, in two measuring circuits.

Circuit one characterises errors in the static mode of measuring. Inertial properties of the primary transducer sensitive element are accounted for in the second circuit through the parameters of the operational part of its transfer function $W_{pt}(p)$, which is regarded as the fraction-rational function of the complex variable p. This type of the block diagram shown in Fig.1 allows for the processes, which form the dynamic error inertial component, to be separated as an independent measuring procedure that corresponds to the dynamic mode of operation of the instrument.

Deviations of pphysical parameters shown in the diagram and the measuring design of the instrument, together with deviations of the parameters, which characterise the adopted method of measuring, can be expressed through a summary indicator, i.e. the deviation of the sensitivity coefficient Δc.

$$\Delta c = c - c_0 , \tag{1}$$

where c - is the actual value of the sensitivity coefficient and c_0 - is the reference value of the sensitivity coefficient.

The presence of deviation Δc leads to a change in static characteristics from the reference function $f_r(x)$. The said change can be defined as an error of static characteristics which is expressed by

$$\Delta f(x) = f_v(x) - f_r(x), \tag{2}$$

where $f_v=f_v(x,q_1,q_2,...,q_n)$ is the actual function of the static characteristics which depends on the measured value x and the actual values of coefficients $q_1,q_2,...,q_n$, each of which is defined by the respective physical parameters of the instrument; $f_r=f_r(x,q_{10},q_{20},...,q_{n0})$ is the reference function of the static characteristic in which $q_{10},q_{20},...,q_{n0}$ are the reference values of the physical parameters of the instrument.

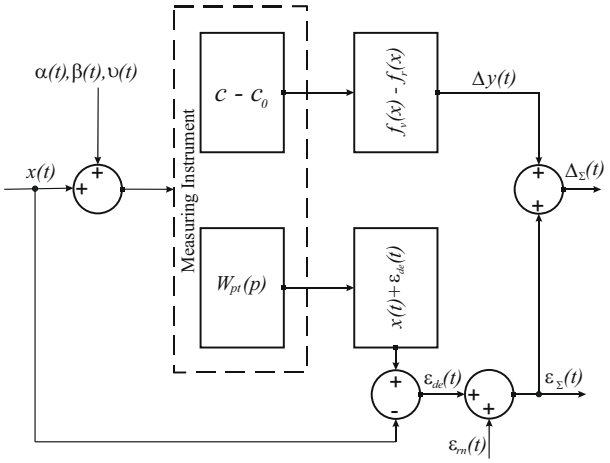

Fig. 1 Dynamic error block diagram

Since the static characteristic is at the end of the measuring instrument metrological circuit containing in itself all deviations of instrument parameters $\Delta q_i=q_i-q_{i0}$, it will be appropriate to express the error in static mode of measuring Δy through the deviation $\Delta f(x)$. On the other hand, the value $\Delta f(x)$ depends not only on the parameters of the measuring instrument, but also on the current values of the measured quantity x. In the dynamic mode of operation, the measured quantity x is a function of time, $x = x(t)$. Accordingly, the error Δy at the output of the first circuit will vary on the basis of the dynamic character of the quantity being measured and, in this sense, be regarded as a function of time, $\Delta y=\Delta y(t)$.

As previously stated, the major part of the summary error $\Delta_\Sigma(t)$ of instruments which measure the parameters of moving objects in the dynamic mode, is due to the deviations of the primary transducer sensitive element that are caused by inertial effects. This is why the formation of this error is structured by means of a separate circuit shown in Fig. 1. This allows us to investigate not only the characteristics of the dynamic error, but also to set up algorithms, methods, and means for its elimination as an independent component. In instruments for measuring the angular position of moving objects, the dynamic character of the measured quantity $x(t)$ and other external effects, $\alpha(t)$, $\beta(t)$, and $\upsilon(t)$, do influence the spatial stability of the sensitive element due to its inertial properties. This leads to the deviation $\varepsilon_{de}(t)$ of the sensitive element from its reference position along the direction of the measuring coordinate, which accrues as an absolute value to the measurement result $x(t)+\varepsilon_{de}(t)$. Deviation $\varepsilon_{de}(t)$ is the basic component of the dynamic error $\varepsilon_\Sigma(t)$. Random noises which are available in the measuring circuit of the instrument are designated in Fig. 1 by means of the component $\varepsilon_{rn}(t)$.

The block diagram shown in Fig. 1 allows the dynamic error characteristics to be investigated as well as algorithms, methods, and means to be devised for elimination of the dynamic error as an independent component. This way, one can devise new intelligent measuring systems whose improved accuracy factors in the dynamic mode of measuring are formed based on the dynamic error elimination in real time.

3. A system for measuring angular deviations of moving objects

The system is designed to measure the roll, pitch, heel, and trim of moving objects (boats, air-crafts, and ground vehicles). It has been developed based on the concept which is defined in the previous section of this study; its block diagram is shown in Fig. 2. The primary transducer consists of a sensitive element and two absolute rotary encoders (ARE) which measure the angular position of the moving object in relation to the vertical in two mutually perpendicular directions. The sensitive element is a physical pendulum with two degrees of freedom. Using the two absolute encoders, the angular deviations of the moving object along the directions of its roll and pitch are measured with regard to the fixed position of the pendulum.

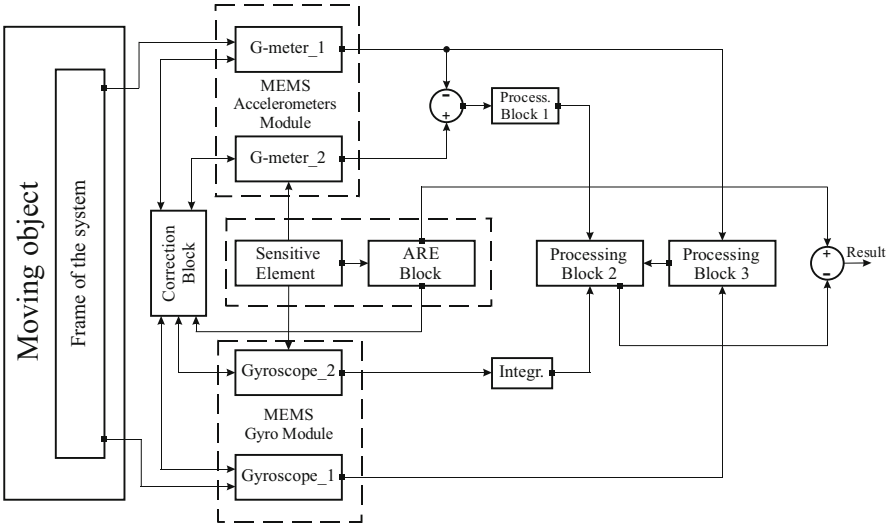

Fig. 2 Block diagram of the measurement system for defining theangular position of moving objects

To ensure high accuracy of the system in the dynamic mode, a correction algorithm which eliminates the dynamic error in real time is used. The principle of operation of the algorithm is based on a hardware-software platform using signals from MEMS accelerometers and gyroscopes.

The body frame $X_bY_bZ_b$ makes movement in relation to the Earth, i.e. the reference frame $X_EY_EZ_E$, so that the relative angular position of the object is defined by the following orientation cosine matrix (Fig.3):

$$M_E^b = \begin{bmatrix} cos\varphi cos\psi & sin\varphi cos\psi & -sin\psi \\ cos\varphi sin\psi sin\theta - & cos\varphi cos\theta + & cos\psi sin\theta \\ -sin\varphi cos\theta & +sin\varphi sin\psi sin\theta & \\ sin\varphi sin\theta + & sin\varphi sin\psi cos\theta - & cos\psi cos\theta \\ +cos\varphi sin\psi cos\theta & -cos\varphi sin\theta & \end{bmatrix}, \quad (3)$$

where ψ, θ, and φ designate the angles of pitch, roll, and yaw of the moving object.

In Figure 3, the sway, surge, and heave of a moving object, which disturb the sensitive element of the primary transducer, are designated as $\eta(t)$, $\xi(t,$ and $\zeta(t),$ respectively. Since the heel and trim of a moving object are time functions of the momentary values of the roll θ and the pitch $\psi,$ they will be, herein after, designated as $\theta(t)$ and $\psi(t)$.

As a result of inertial forces and moments that have been generated by the movement and oscillations of the moving object, the sensitive element will deviate from its vertical position. The angular deviation of the sensitive element frame $X_{se}Y_{se}Z_{se}$ with regard to the system $X_EY_EZ_E$ is defined in Fig. 3 by means of the angles ε_{de}^{ψ} and $\varepsilon_{de}^{\theta}$, and the orientation cosine matrix will be

$$M_E^{se} = \begin{bmatrix} cos\,\varepsilon_{de}^{\psi} & 0 & -sin\,\varepsilon_{de}^{\psi} \\ sin\,\varepsilon_{de}^{\psi} sin\,\varepsilon_{de}^{\theta} & cos\,\varepsilon_{de}^{\theta} & cos\,\varepsilon_{de}^{\psi} sin\,\varepsilon_{de}^{\theta} \\ sin\,\varepsilon_{de}^{\psi} cos\,\varepsilon_{de}^{\theta} & -sin\,\varepsilon_{de}^{\theta} & cos\,\varepsilon_{de}^{\psi} cos\,\varepsilon_{de}^{\theta} \end{bmatrix}. \tag{4}$$

The sensitive element movement, which is produced by the impact of inertial forces and moments, can be defined by the following system of differential equations:

$$\begin{aligned} &\ddot{\varepsilon}_{de}^{\theta}(t) + 2b_1\dot{\varepsilon}_{de}^{\theta}(t) + \omega_{01}^2\varepsilon_{de}^{\theta}(t) = \alpha_1\left[\ddot{\eta}(t) + x\ddot{\varphi}(t) - z\ddot{\theta}(t)\right]; \\ &\ddot{\varepsilon}_{de}^{\psi}(t) + 2b_2\dot{\varepsilon}_{de}^{\psi}(t) + \omega_{02}^2\varepsilon_{de}^{\psi}(t) = \alpha_2\left[\ddot{\xi}(t) + y\ddot{\varphi}(t) + z\ddot{\theta}(t)\right], \end{aligned} \tag{5}$$

where b_1 and b_2 - are the coefficients that determine the attenuation of pendulum oscillations along the coordinates Y_{se} and X_{se}; x, $y,$ and z are the coordinates defining the position of the instrument with regard to the centre of rotation of the object ω_{01} and ω_{02} are the inherent frequencies of the pendulum along the directions of coordinates Y_{se} and X_{se}; $\alpha_1=\omega_{01}/g$; $\alpha_2=\omega_{02}/g$.

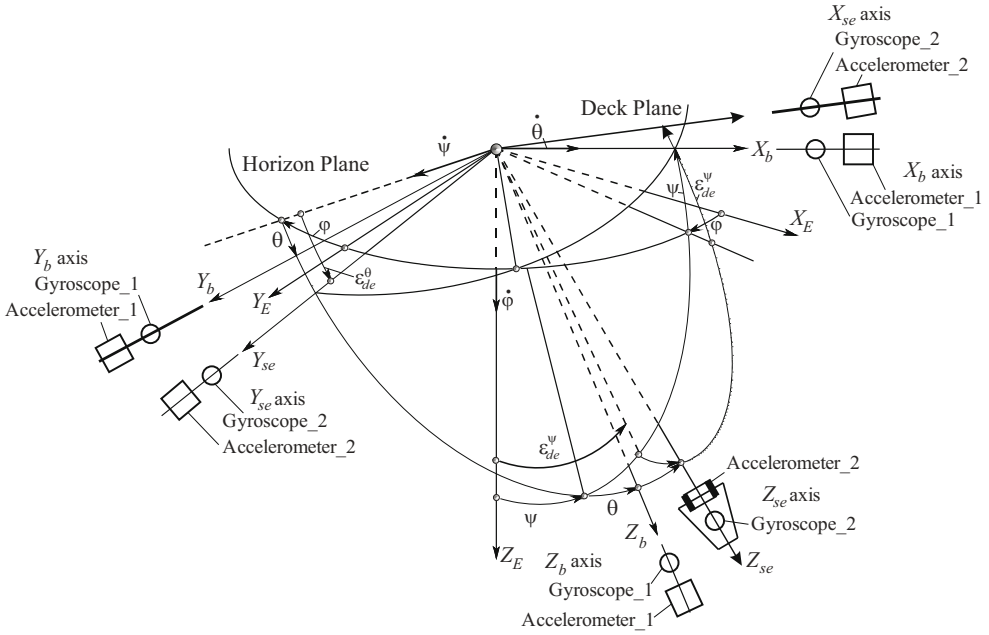

Fig. 3 Angular offset of coordinate systems

The values of angular deviations $\varepsilon_{de}^{\psi}(t)$ and $\varepsilon_{de}^{\theta}(t)$ are equal to the dynamic error components $\varepsilon_{de}(t)$ when measuring the pitch and roll of the object. The definition of the

current values of these two dynamic error components obtained through the measuring system presented in this study is based on the measurement-calculation approach. A sensor configuration consisting of two blocks with MEMS sensors is used to implement the measurement part (Fig.2). Block one consists of two identical 3-axis MEMS based gyroscopes. One of the gyros is mounted on the instrument body so that its measuring axes coincide with those of the frame $X_bY_bZ_b$, whereas the second one is fixed on the physical pendulum and its axes are oriented in accordance with the axes of the frame $X_{se}Y_{se}Z_{se}$. Measuring block two is designed on the basis of two identical 3-axis MEMS g-meters, which are mounted in the same way as the two gyros, i.e. on the instrument body and on the pendulum, with the measuring axes coinciding with the axes of $X_bY_bZ_b$ and $X_{se}Y_{se}Z_{se}$. G-meter 2(two) is sensitive to all accelerations acting on g-meter 1(one) as well as to accelerations generated by the angular oscillation of the pendulum. This is the reason why the difference in the readings of both g-meters will be proportional to the functions $\ddot{\varepsilon}^{\psi}_{de}(t)$ and $\ddot{\varepsilon}^{\theta}_{de}(t)$. The received signals are in fact equal to the tangential accelerations at the spot where g-meter 2(two) is mounted, thereby, the tangential accelerations are transformed in the "processing block 1" into angular accelerations and, following a double integration, are then passed onto the "processing block 2". With this accelerometric approach to dynamic error measurement, additional disturbances generated by secondary accelerations of the kind $\ddot{\zeta}(t)\cdot\varepsilon^{\psi}_{de}(t)$ and $y\cdot\ddot{\psi}(t)\cdot\varepsilon^{\psi}_{de}(t)$ are accrued to useful signals. However, these disturbances occur as small quantities of the second order and therefore their influence is negligible. Along with that, the signal received from the differential connection of two identical g-meters provides far more accurate and reliable data than those coming from just one such g-meter. Thus, it is possible to eliminate some methodical errors of MEMS g-meters such as gravitation errors.

In this study the current values of dynamic errors $\varepsilon^{\psi}_{de}(t)$ and $\varepsilon^{\theta}_{de}(t)$ are defined on the basis of two 3×1 vectors $\boldsymbol{\rho}^{\boldsymbol{\psi}}$ and $\boldsymbol{\rho}^{\boldsymbol{\theta}}$. The elements of the vectors $\boldsymbol{\rho}^{\boldsymbol{\psi}}$ and $\boldsymbol{\rho}^{\boldsymbol{\theta}}$ are formed by the data received from gyro 2, "processing block 1" and "processing block 3". The result at the output of the "processing block 3" is obtained by the measurement-calculation method which contains a supposition that the information about current dynamic error values can be obtained through the theoretical model of physical pendulum dynamics, whose input vector is obtained as a result of measurement. The said theoretical model is based on equations (5), the information on the current values of quantities on the right side of these differential equations is received from gyro 1 and g-meter 1.

The final evaluation of dynamic error components $\varepsilon^{\psi}_{de}(t)$ and $\varepsilon^{\theta}_{de}(t)$ is obtained at the output of "processing block 2" by means of which the two absolute rotary encoders correct the currently measured values of the angles of roll, pitch, heel, and trim. The principle of "processing block 2" operation is given due consideration in the next section of this study.

A "correction block" has been provided to compensate errors of MEMS sensors in the measuring system circuit. For example, the error resulting from the gyro bias is eliminated by accepting as reference values the readings of the two absolute rotary encoders at those moments in which g-meter 2 recognizes the condition of rest of the primary transducer's sensitive element.

4. Processing algorithm model

The algorithm model implemented in the "processing block 2" is developed for defining the optimum evaluation of the dynamic error components $\varepsilon^{\psi}_{de}(t)$ and $\varepsilon^{\theta}_{de}(t)$ according to the requirement for minimum mean squared deviation of the current and previous evaluations

which alter the state of vectors ρ^{ψ} and ρ^{θ}. This algorithm considerably increases the measuring system accuracy because it is based on the actual model of the sensitive element dynamics and the analysis of each new measurement in the time sequence.

Figure 4 shows how the algorithm works. The current values of measurement-calculation vectors ρ^{ψ} and ρ^{θ} are fed into the "processing block 2". Data is recorded in the matrices N×3,

$$A_{\psi} = \begin{bmatrix} a_{11}^{\psi} & a_{12}^{\psi} & a_{13}^{\psi} \\ a_{21}^{\psi} & a_{22}^{\psi} & a_{23}^{\psi} \\ a_{31}^{\psi} & a_{32}^{\psi} & a_{33}^{\psi} \\ \vdots & \vdots & \vdots \\ a_{N1}^{\psi} & a_{N2}^{\psi} & a_{N3}^{\psi} \end{bmatrix}; \quad A_{\theta} = \begin{bmatrix} a_{11}^{\theta} & a_{12}^{\theta} & a_{13}^{\theta} \\ a_{21}^{\theta} & a_{22}^{\theta} & a_{23}^{\theta} \\ a_{31}^{\theta} & a_{32}^{\theta} & a_{33}^{\theta} \\ \vdots & \vdots & \vdots \\ a_{N1}^{\theta} & a_{N2}^{\theta} & a_{N3}^{\theta} \end{bmatrix}, \tag{6}$$

for the vectors ρ^{ψ} and ρ^{θ}, respectively.

The data received from gyro 2, "processing block 1" and "processing block 3" are recorded in each of the columns of the matrices A_{ψ} and A_{θ}. The data from gyro 2 are recorded in the first column, containing the elements $a_{i,1}^{\psi,\theta}, i = 1,...,N$. The data from "processing block 1" and "processing block 3" are recorded in the second and third columns, containing the elements $a_{i,2}^{\psi,\theta}, i = 1,...,N$ and $a_{i,3}^{\psi,\theta}, i = 1,...,N$.

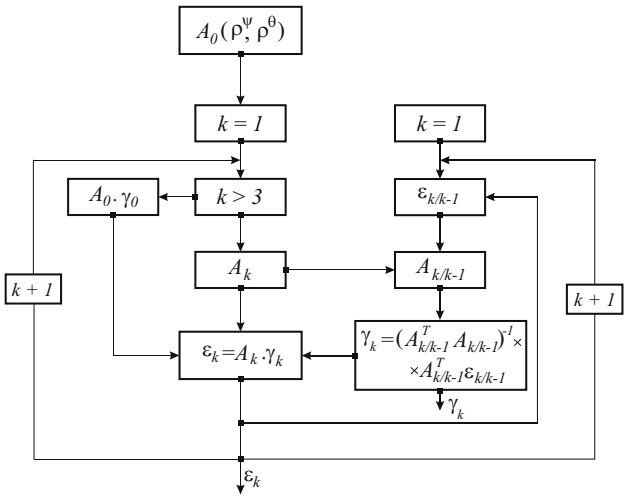

Fig. 4 Algorithm of the processing block 2

The algorithm shown in Fig. 4 is derived from the equation below:

$$\hat{\varepsilon} = A \cdot \gamma + \delta, \tag{7}$$

where $\hat{\varepsilon}$ is the 3×1 vector that contains the dynamic error $\varepsilon_{de}(t)$ values at the current and the two previous moments of time; A is the matrix with dimensions 3×3; γ is the 3×1 vector whose elements determine the rate of veracity of each of the current values of vector elements ρ^{ψ} and ρ^{θ}; δ is the 3×1 vector whose elements determine the values of the random component in equation (7).

The algorithm from Fig. 4 is executed in parallel for each of the two measuring coordinates; for this reason, indices ψ and θ will be skipped when considering the mathematical model. Equation (7) can be written in its extended form in the following way:

$$\begin{bmatrix} \varepsilon_{k-2} \\ \varepsilon_{k-1} \\ \varepsilon_{k} \end{bmatrix} = \begin{bmatrix} a_{k-2,1} & a_{k-2,2} & a_{k-2,3} \\ a_{k-1,1} & a_{k-1,2} & a_{k-1,3} \\ a_{k,1} & a_{k,2} & a_{k,3} \end{bmatrix} \begin{bmatrix} \gamma_{1,k} \\ \gamma_{2,k} \\ \gamma_{3,k} \end{bmatrix} + \begin{bmatrix} \delta_{1,k} \\ \delta_{2,k} \\ \delta_{3,k} \end{bmatrix}. \tag{8}$$

In (8), the vector for the current state of the sensitive element is marked with the index *k*. In solving the task for optimality, it is necessary that for each current state, there should be identified such values for the vector $\boldsymbol{\gamma}$ whereby the elements of the random component $\boldsymbol{\delta}$ are to have their minimum. This study puts forward the hypothesis that the vector $\boldsymbol{\delta}$ has zero expectation, i.e. $E(\boldsymbol{\delta})=0$. In practice, it could be accepted that the elements of matrices (6) accrue as a result of the measurement done within the limits of a comparatively short period of time and that in themselves they are a homogeneous time set. In addition, it is possible to affirm (with sufficient accuracy for practical solutions) that the processes in consideration are stationary random functions of time. Accordingly, it could be expected that the vector $\boldsymbol{\delta}$ has uncorrelated coordinates of identical dispersion σ^2. With such hypothesis, the correlation matrix of the random component $\boldsymbol{\delta}$ would feature the following simple structure [27, 28]:

$$\boldsymbol{E}\left(\boldsymbol{\delta}\cdot\boldsymbol{\delta}^{\boldsymbol{T}}\right)=\boldsymbol{\sigma}^{2}\cdot\boldsymbol{I}\,, \tag{9}$$

where $\boldsymbol{I}$ is the identity matrix with dimensions 3×3.

The optimal values of the elements of $\boldsymbol{\gamma}$ are equal to those values at which the sum of the squared deviations $\boldsymbol{\delta}$ has a minimum. The sum of the squares of $\boldsymbol{\delta}$ is determined by the equality below:

$$\boldsymbol{\delta}^{T}\boldsymbol{\delta}=\left(\hat{\boldsymbol{\varepsilon}}-A\cdot\boldsymbol{\gamma}\right)^{T}\cdot\left(\hat{\boldsymbol{\varepsilon}}-A\cdot\boldsymbol{\gamma}\right). \tag{10}$$

Finding this minimum is identical with the setting to zero of the first derivative on the right side of (10) in relation to $\boldsymbol{\gamma}$, which leads to a system of normal equations

$$A^{T}\cdot A\cdot\boldsymbol{\gamma}=A^{T}\cdot\hat{\boldsymbol{\varepsilon}}\,. \tag{11}$$

The solution of this equation is one and only and it is obtained as

$$\boldsymbol{\gamma}=\left(A^{T}\cdot A\right)^{-1}\cdot A^{T}\cdot\hat{\boldsymbol{\varepsilon}}\,. \tag{12}$$

As one can see from Fig. 4, the iterative process for defining the current values of evaluations $\hat{\boldsymbol{\varepsilon}}$ of the dynamic error is divided into two cycles: a cycle for updating the $\hat{\boldsymbol{\varepsilon}}$ evaluations and a cycle for updating coefficients of the matrix $\boldsymbol{\gamma}$, both of which determine the level of veracity. For the purpose of reducing the amount of calculations, the vector of state $\hat{\boldsymbol{\varepsilon}}$ and the vector of gain $\boldsymbol{\gamma}$ are updated separately by using one and the same matrix $A_{k/k-1}$.

Input data obtained by measurement and calculation and put in order in the vectors $\boldsymbol{\rho}^{\boldsymbol{\psi}}$ and $\boldsymbol{\rho}^{\boldsymbol{\theta}}$ are fed into the buffer $A_0(\rho^{\psi},\rho^{\theta})$ whose initialization is synchronized with the structure and the way of updating the matrix A_k. The latter is a 3×3 matrix which is organized according to the logic of the model (8). The actual evaluation value $\hat{\boldsymbol{\varepsilon}}$ of the dynamic error in the current cycle k is derived from the element ε_k. With $k\leq 3$, evaluations $\hat{\boldsymbol{\varepsilon}}$ are obtained by multiplication of unfinished matrices A_0 by the vector-column $\boldsymbol{\gamma}_0=\left[1\quad 0\quad 0\right]^T$, which means that in these particular cases priority is given to the measurement vector coming from gyro 2.

5. Experiment and results

To prove the veracity of the proposed measurement approach experimental investigations have been conducted on the special purpose prototype of the measurement system. A simulation stand, i.e., a parallel manipulator (hexapod) based on the Stuart platform has been used to carry out the investigations (Fig. 5).

The efficient mechanical components of the hexapod allow motion generation along three angular and three linear coordinates with a wide range of displacement and a wide range of variation in kinematic parameters. The reference properties of the simulation stand movements are proved by the necessary calibration certificates. This allows the measurements in the conducted research to be referred to a common traceable reference. Manipulator User Interface presents a wide range of possibilities for the modelling and control of harmonic, poly-harmonic and random oscillations on its working plate both individually, in accordance with each of the levels of freedom, and in combined movement.

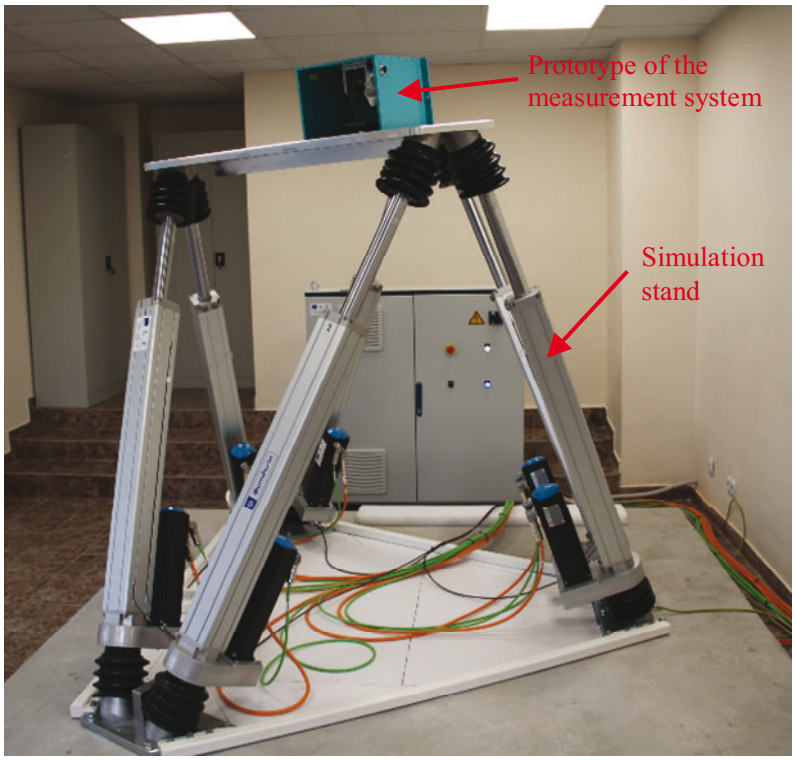

Fig. 5 Simulation stand and a prototype of the measurement system

The prototype of the measurement system is designed on the basis of the block diagram shown in Fig. 2 and the model presented in point 3. The absolute rotary encoders are mounted on the main measuring axes; they register the rotation angles of a moving object relative to the vertical modelled by the physical pendulum. (Fig. 6). The application of differential parallel scanning of each bit of the rotating scale in Gray code eliminates the errors due to interferences and provides a wide operating temperature range. Absolute encoders are characterised by their high accuracy, high noise immunity, fast response, wide range of supply voltage, and small size. In this particular case, the absolute encoders of 2^{13} bit resolution are used. An additional bit is provided in the encoders. It is analogous to the least-significant one but dephased by 90 electrical degrees. This enables the increase in the resolution to 2^{16} bits by analogue interpolation. The said prototype features two ADXL313 g-meters with a measurement range of ±4g and a noise level of $150\,\mu g/\sqrt{Hz}$; it also features

two ITG-3200 gyros with a measurement range of ±2000 deg/s and sensitivity of 14.375 LSBs/deg/s. The proposed processing algorithm for obtaining the time-related sequential evaluations of the dynamic error operates with a renewal frequency of 20 Hz.

Figures 7, 8, and 9 show the results of conducted experiments to illustrate the quality of performance of the proposed measurement system. The results of the operation of the system when measuring the heel without including the algorithm for the elimination of the dynamic error proposed in this paper are shown in Fig. 7b. Figure 7a shows the reference motions generated by the simulation stand which represent harmonic angular oscillations about the X_b axis. In Figure 7b, the signal from the absolute rotary encoder measuring the heel is marked with $\theta_{ARE}(t)$.

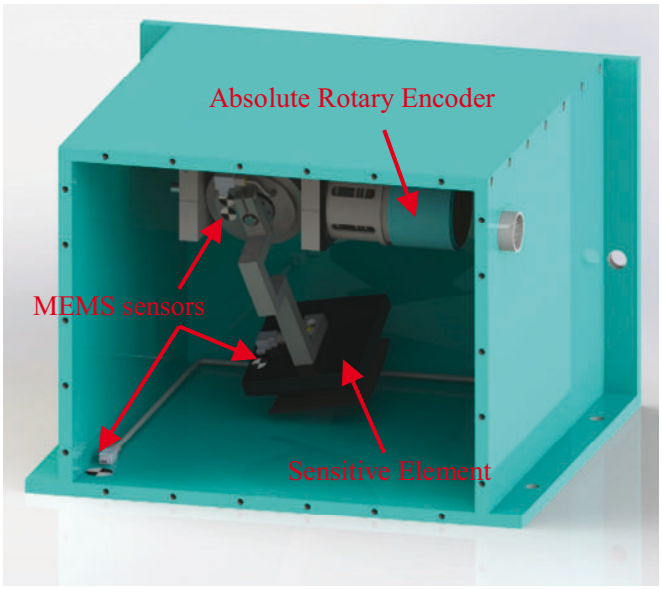

Fig. 6 Prototype of a system for measuring the roll, pitch, heel, and trim of moving objects

It can be seen that the signal $\theta_{ARE}(t)$ differs substantially from the signal $\theta_{ref}(t)$ which defines the reference movement of the simulation stand. The summary error $\Delta_{\Sigma}^{\theta}(t)$ of the investigated prototype when the system operates in the dynamic mode of measurement without a sensor configuration processing block can be determined by the difference between the two signals, $\Delta_{\Sigma}^{\theta}(t) = \theta_{ARE}(t) - \theta_{ref}(t)$. This model of summary error $\Delta_{\Sigma}^{\theta}(t)$ comprises not only the basic component $\varepsilon_{de}^{\theta}(t)$ along with all other dynamic error components $\varepsilon_{\Sigma}^{\theta}(t)$, but also all instrumental and methodical errors expressed by the $\Delta y(t)$ function (Fig. 1). It is evident that in this mode of the system operation, the summary error can reach high values. In this particular case, the maximum value of the summary error $\Delta_{\Sigma}^{\theta}(t)$ when measuring the heel is 19°, whereas the standard deviation from the reference curve is $\sigma_{\Delta}^{\theta} = 6^{o}$. In order to define the quantitative ratio between the summary error $\Delta_{\Sigma}^{\theta}(t)$ and the basic component $\varepsilon_{de}^{\theta}(t)$ of the dynamic error resulting from the deviations of the sensitive element from the vertical, the functions of the summary and basic component errors are shown in Figure 7.

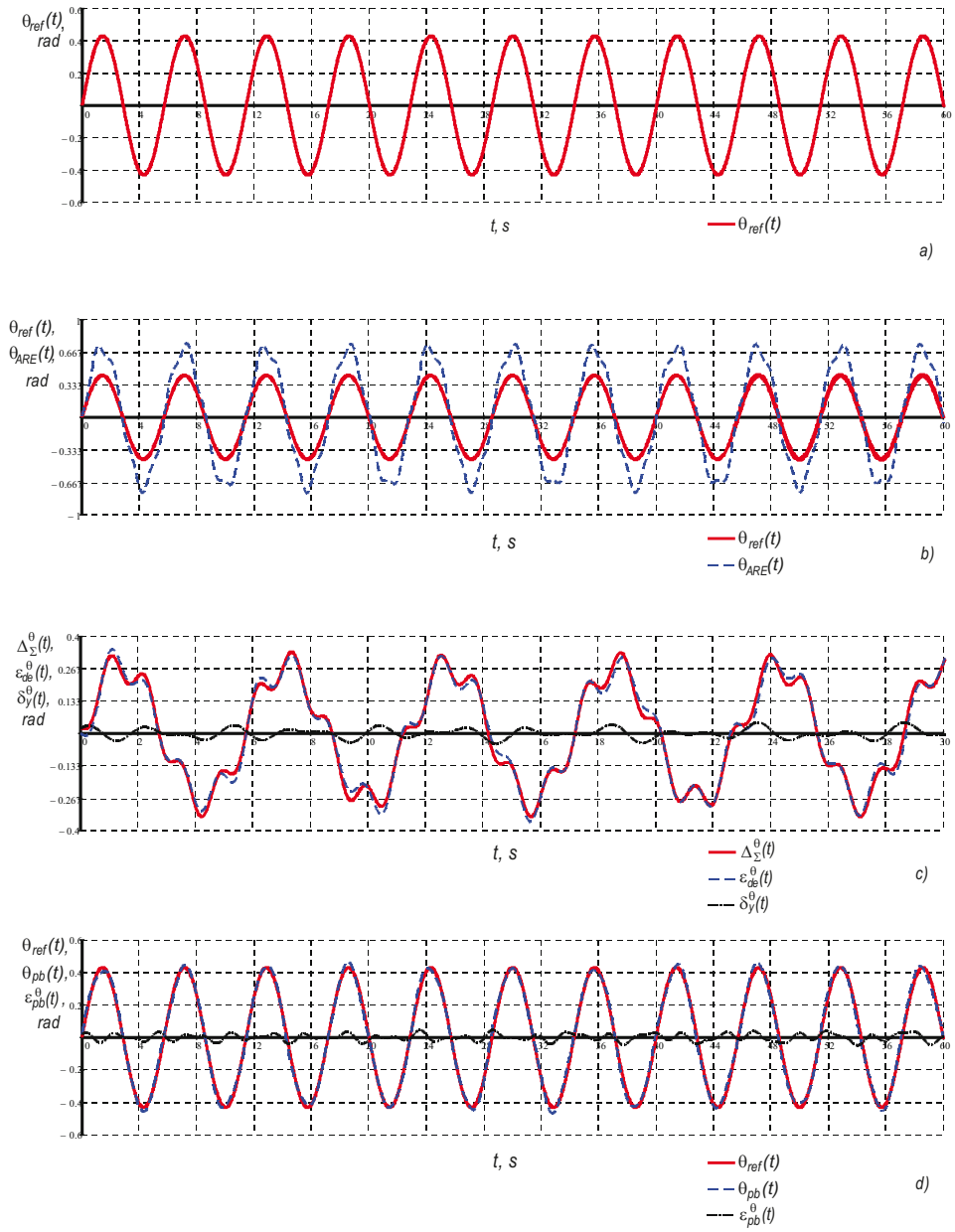

Fig. 7 Results of investigation carried out in the harmonic mode of operation

The signal $\varepsilon_{de}^{\theta}(t)$ comes from the output of the processing block with the sensor configuration of the roll channel and the function $\delta_y^{\theta}(t) = \Delta_{\Sigma}^{\theta}(t) - \varepsilon_{de}^{\theta}(t)$ is marked with $\delta_y^{\theta}(t)$. The function $\delta_y^{\theta}(t)$ allows the influence of all components of the summary error $\Delta_{\Sigma}^{\theta}(t)$ without the basic component $\varepsilon_{de}^{\theta}(t)$ on the formation of the summary error to be accounted for. From Fig. 7 one can see that the relative share of the function $\delta_y^{\theta}(t)$ values does not exceed 12% of the summary error $\Delta_{\Sigma}^{\theta}(t)$. Similar results have been observed when investigating other modes of movement of the simulation stand, including measurements along the roll channel as well as measurements along the pitch channel. Therefore, the accuracy of measurement in the dynamic mode is primarily determined by the values of the inertial component of the dynamic error $\varepsilon_{de}(t)$, which results from accelerations occurring during the movement of moving objects.

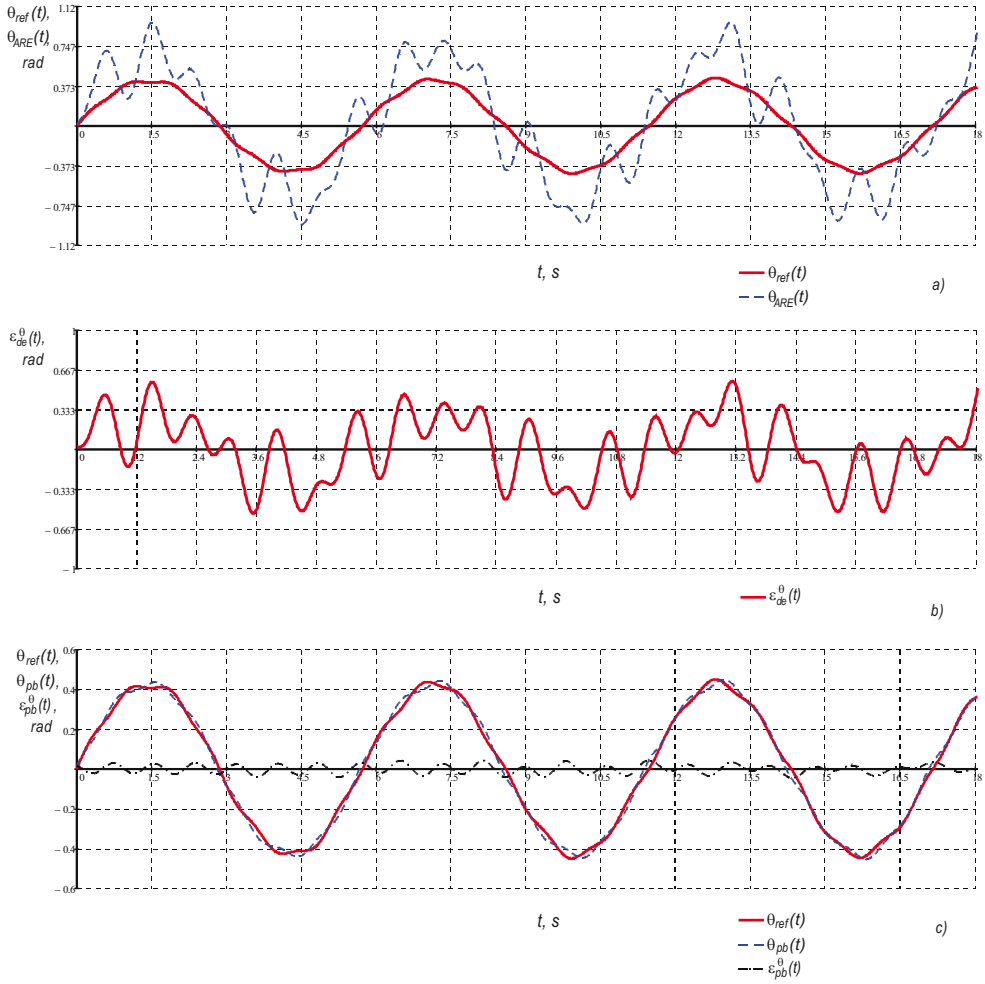

Fig. 8 Results of investigation carried out in the poly-harmonic mode of operation

The employment of the processing block with the sensor configuration proposed in this study enhances the measurement accuracy significantly, which is shown in Fig. 7d. This figure shows the curves that define the reference movement of the simulation stand $\theta_{ref}(t)$ and the signal coming from the output of the measuring system $\theta_{pb}(t)$ operating with the processing block. A graphical representation of the dynamic error defined by the equality $\varepsilon^{\theta}_{pb}(t) = \theta_{pb}(t) - \theta_{ref}(t)$ is shown in the same figure. In this case the maximum value of the error $\varepsilon^{\theta}_{pb}(t)$ when measuring the heel is 52', whereas the standard deviation from the reference curve is $\sigma^{\theta}_{pb} = 11'$.

When studying dynamic accuracy of the system in the poly-harmonic operation mode of the simulation stand, a significant increase in the maximum value of the basic component of the dynamic error $\varepsilon^{\theta}_{de}(t)$ (Fig. 8b) is observed. This is due to the additional dynamic response of the sensitive element to the second and third inertial components of the signal $\theta_{ref}(t)$ defining the reference motion of the simulation stand. The signal $\theta_{ref}(t)$ is formed by adding two higher frequency components (the continuous curve in Fig. 8a) to the harmonic signal from Fig. 7a. The maximum value of the dynamic error $\varepsilon^{\theta}_{de}(t)$ in this particular case exceeds by 31% the respective dynamic error obtained from the investigation carried out in the harmonic operation mode of the simulation stand. However, the increase in the maximum

value of the dynamic error $\varepsilon_{pb}^{\theta}(t)$ is considerably smaller and does not exceed 10% of the value of the respective error in the harmonic mode of investigation with the sensor configuration processing block.

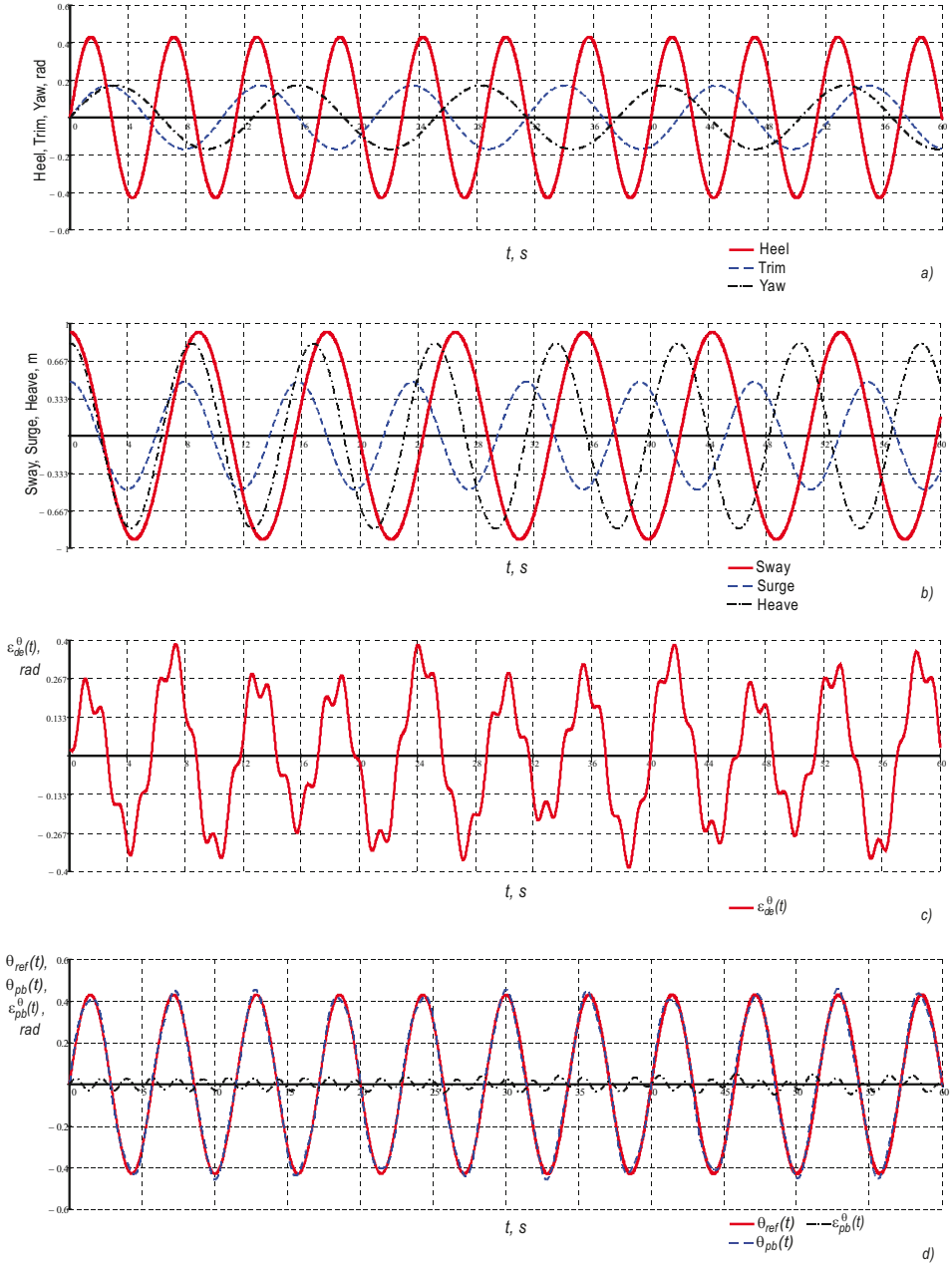

Fig. 9 Results of investigation carried out in a combined mode of operation

How inertial effects, which result from the oscillation motions in all six degrees of freedom of the moving object, influence the dynamic accuracy of the measurement system is studied in the third dynamic model. Figure 9 shows the reference angular motions, modelled by the simulation stand, which include: the heel (continuous curve), the trim (broken curve), and the yaw (dotted curve). The curves showing the translational motions (sway, surge, and heave) are shown in Fig. 9b. It can be seen that the maximum value of the dynamic error $\varepsilon_{de}^{\theta}(t)$ exceeds the respective dynamic error from investigations in the harmonic mode of operation by no more than 18% (Fig. 9c), whereas, in the operation mode with the sensor configuration processing block, the maximum value of the error $\varepsilon_{pb}^{\theta}(t)$ is 52' (Fig. 9d). Even

when tested in harsher conditions of operation, the maximum value of the error $\varepsilon_{pb}^{\theta}(t)$ does not exceed 1°.

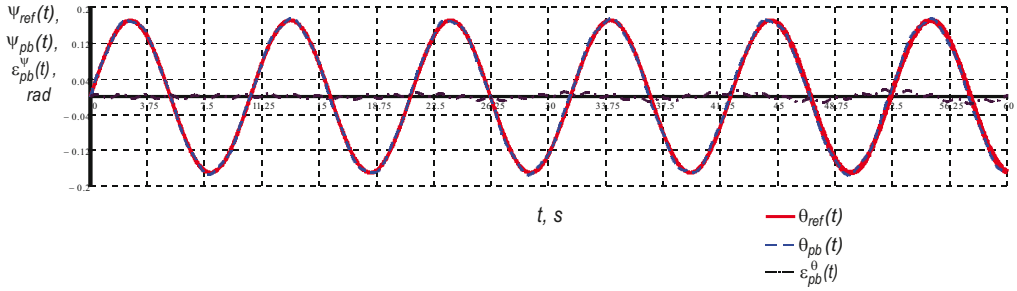

Fig. 10 Results of a study on the accuracy of measurements of the trim in a combined mode of operation

Similar results are obtained when examining the accuracy of the measurement of trim. The results of measuring the trim during operation of the system with the included algorithm for the dynamic error elimination are presented in Fig.10. The investigations were conducted during oscillations of the simulation stand in all six degrees of freedom; they are presented graphically in Fig. 9a and Fig. 9b. The error $\varepsilon_{pb}^{\psi}(t)$ in measuring the trim is determined by the equality $\varepsilon_{pb}^{\psi}(t) = \psi_{pb}(t) - \psi_{ref}(t)$, where $\psi_{ref}(t)$ is the function defining the reference values of the trim of the simulation stand, and $\psi_{pb}(t)$ is the signal received at the output of the measuring system. The investigations show that the maximum value of the error $\varepsilon_{pb}^{\psi}(t)$ in measuring the trim is 48', and the standard deviation, determined relative to the reference curve, is $\sigma_{pb}^{\psi} = 10'$.

6. Conclusions

A novel method for developing systems for the measurement of angular orientation of moving objects has been proposed. The concept of the method is based on the elimination of the dynamic error major component resulting from the deviations of the primary transducer sensitive element from its reference position due to inertial effects.

The elimination of the dynamic error is based on the mathematical model presented in this study. The mathematical model makes it possible to determine the best estimate of the dynamic error $\hat{\boldsymbol{\varepsilon}}$, based on minimizing the variance of a random component, which defines the difference between $\hat{\boldsymbol{\varepsilon}}$ and the measurement-computational model. The developed model makes it possible through the measuring computing platform to cover previous and current values of a wide range of quantities involved in the formation of the dynamic error. Thus, appropriate algorithms for determining the dynamic error relative to reference dynamic models can be created.

Because of the simplified design of the sensitive element, measurement instruments of very small instrumental error could be developed using this method. Based on the proposed method, a measurement system for defining the roll, pitch, heel, and trim of moving objects has been developed. High dynamic accuracy of the system is guaranteed by the measurement-calculation platform whose output vector is formed by the data coming from the sensor configuration, which consists of two blocks with MEMS sensors. The output vector which contains the dynamic error current values is obtained by means of an algorithm which is based on the mean squared deviation criterion.

The results of experiments are presented in this study. The experiments are carried out with the help of a hexapod, developed on the basis of the Steward platform and produced by the company "Symetrie". The characteristics of the prototype built for this purpose of the measuring system presented in this paper are studied. The performed experiments proved the effectiveness of the proposed method.

Acknowledgements

This research was supported by the European Regional Development Fund within the OP "Science and Education for Smart Growth 2014 - 2020", Project CoC "Smart Mechatronic, Eco- And Energy Saving Systems And Technologies", № BG05M2OP001-1.002-0023.

REFERENCES

[1] Song L., Chen Z., Mao Y., Dong Z., Xiang Z., Error Mitigation Algorithm Based on Bidirectional Fitting Method for Collision Avoidance of Unmanned Surface Vehicle, *Polish Maritime Research* **2018**, 25 (4), 13-20. https://doi.org/10.2478/pomr-2018-0127

[2] De Marco, D., Dolara, A., Longo, M., A review on dynamic wireless charging systems, In *2019 IEEE Milan PowerTech* **2019**, June, 1-5. https://doi.org/10.1109/PTC.2019.8810831

[3] Kadem, K., Cheriet, F., Laboure, E., Bensetti, M., Le Bihan, Y., Debbou, M. Sensorless Vehicle Detection for Dynamic Wireless Power Transfer. In *2019 21st European Conference on Power Electronics and Applications (EPE'19 ECCE Europe)* **2019**, September, P-1. https://doi.org/10.23919/EPE.2019.8915150

[4] Liu, Z., Ship Course Keeping Using Different Sliding Mode Controllers, *Transactions of FAMENA* **2019**, 43(2), 49-60. https://doi.org/10.21278/TOF.43204

[5] Tomczyk, K., Procedure Proposal for Establishing the Class of Dynamic Accuracy for Measurement Sensors Using Simulation Signals with One Constraint, *Measurement* **2021**, 178. https://doi.org/10.1016/j.measurement.2021.109367

[6] Yurasova, E. V., Rusanova, A. C., Implementation of the Genetic Algorithmfor Correcting the Dynamic Error of the Measuring Systems, In *2020 Global Smart Industry Conference (GloSIC)* **2020**, November, 240-245. https://doi.org/10.1109/GloSIC50886.2020.9267875

[7] Hessling, J. P., A novel method of estimating dynamic measurement errors, *Measurement Science and Technology* **2006**, 17(10), 2740-2750. https://doi.org/10.1088/0957-0233/17/10/028

[8] Hessling, J. P., A novel method of evaluating dynamic measurement uncertainty utilizing digital filters, *Measurement Science and Technology* **2009**, 20(5). https://doi.org/10.1088/0957-0233/20/5/055106

[9] Tomczyk, K., Piekarczyk, M., Sokal, G., Radial basis functions intended to determine the upper bound of absolute dynamic error at the output of voltage-mode accelerometers, *Sensors* **2019**, 19(19). https://doi.org/10.3390/s19194154

[10] Dichev, D., Koev, H., Bakalova, T., Louda, P., A model of the dynamic error as a measurement result of instruments defining the parameters of moving objects, *Measurement Science Review* **2014**, 14(4), 183-189. https://doi.org/10.2478/msr-2014-0025

[11] Sun, F., Guo, C., Gao, W., Li, B., A new inertial measurement method of ship dynamic deformation, In *2007 International Conference on Mechatronics and Automation* **2007**, August, 3407-3412. https://doi.org/10.1109/ICMA.2007.4304110

[12] Bryne, T. H., Rogne, R. H., Fossen, T. I., Johansen, T. A., Attitude and heave estimation for ships using mems-based inertial measurements, *IFAC-PapersOnLine* **2016**, 49(23), 568-575. https://doi.org/10.1016/j.ifacol.2016.10.496

[13] Uharek, S., Cura-Hochbaum, A., The influence of inertial effects on the mean forces and moments on a ship sailing in oblique waves Part B: Numerical prediction using a RANS code, *Ocean Engineering* **2018**, 165, 264-276. https://doi.org/10.1016/j.oceaneng.2018.07.002

[14] Rogne, R. H., Johansen, T. A., Fossen, T. I., On attitude observers and inertial navigation for reference system fault detection and isolation in dynamic positioning, In *2015 European Control Conference (ECC)* **2015**, July, 3665-3672. https://doi.org/10.1109/ECC.2015.7331100

[15] Danilov, A. T., A Gyroscopic Measuring System for Parameters of Moving Objects. *Problems of Special Machinebuilding Magazine* **2001**, 4 (1), 178-181.

[16] Ivanov, Y. V., Autonomous Sensors for Heal, Trim and Vertical Displacements of Underwater and Above-Water Objects. *Sensors and Systems Magazine* **2000**, 5 (1), 33-37

[17] Pelpor, D. S., Orientation and Stabilization Gyroscopic Systems. *Mashinostroene* **1982**, Moscow.

[18] Yang, H., Zhao, Y., Li, M., Wu, F. The static unbalance analysis and its measurement system for gimbals axes of an inertial stabilization platform. *Metrol. Meas. Syst*. **2015**, 22(1), 51–68. https://doi.org/10.1515/mms-2015-0002

[19] Kok, M., Wahlström, N., Schön, T. B., Gustafsson, F., MEMS-based inertial navigation based on a magnetic field map, In *2013 IEEE International Conference on Acoustics, Speech and Signal Processing* **2013**, May, 6466-6470. https://doi.org/10.1109/ICASSP.2013.6638911

[20] Rogne, R., Bryne, T., Fossen, T., Johansen, T., Redundant MEMS-based inertial navigation using nonlinear observers, *Journal of Dynamic Systems, Measurement, and Control* **2018**, 140(7). https://doi.org/10.1115/1.4038647

[21] Chatterjee, G., Latorre, L., Mailly, F., Nouet, P., Hachelef, N., Oudea, C., MEMS based Inertial Measurement Units, In *2015 Symposium on Design, Test, Integration and Packaging of MEMS/MOEMS (DTIP)* **2015**, April, 1-5. https://doi.org/10.1109/DTIP.2015.7160966

[22] Du, B., Song, J., Shi, Z., An anomaly diagnosis method for redundant inertial measurement unit and its application with micro-electro-mechanical system sensors, *Applied Sciences* **2019**, 9(8). https://doi.org/10.3390/app9081606

[23] Kvedaras, R., Kvedaras, V., Ustinavičius, T., Masiulionis, R., Digital Signal Processing Algorithm for Measurement of Settling Time of High-Resolution High-Speed DACs, *Measurement Science Review* **2019**, 19(3), 86-92. https://doi.org/10.2478/msr-2019-0014

[24] Karadzhov, T., Pulov, D., Angelov, N., Contactless measuring of temperature with differential photo receiver, In *ENVIRONMENT. TECHNOLOGIES. RESOURCES. Proceedings of the International Scientific and Practical Conference* **2019**, June, 3, 101-104. https://doi.org/10.17770/etr2019vol3.4132

[25] Diakov, D., Radev, H., Vassilev, V., Nikolova, H., Measurement system based on virtual reference axis for evaluation form and location of surfaces and axes of rotary details, In *Journal of Physics: Conference Series* **2019**, November, 1379(1). https://doi.org/10.1088/1742-6596/1379/1/012074

[26] Pencheva, T., Pulov, D., Gyoch, B., Nenkov, M., Design of CCD Optical System for Thermal IR Spectral Region, In *2006 29th International Spring Seminar on Electronics Technology* **2006**, May, 173-178. https://doi.org/10.1109/ISSE.2006.365380

[27] Sveshnikov, A. A., Applied methods of the theory of random functions, *Elsevier* **2014**.

[28] Ventzel, E. S., Ovcharov, L. A., Random Processes Theory and its Engineering Applications, *Vishaia shkola* **2000**, Moscow.

Submitted: 18.4.2021

Accepted: 22.10.2021

Dimitar Dichev*
Iliya Zhelezarov
Faculty of Mechanical and Precision Engineering,
Technical University of Gabrovo,
Hadzhi Dimitar Str. 4, 5300 Gabrovo,
Bulgaria

Nikolay Madzharov
Faculty of Electrical Engineering and Electronics,
Technical University of Gabrovo
Hadzhi Dimitar Str. 4, 5300 Gabrovo,
Bulgaria

*Corresponding author:
dichevd@abv.bg